



HAL
open science

Modélisation non linéaire et optimisation de la gamme dynamique des nanocapteurs résonants

Najib Kacem, Sébastien Hentz, Sébastien Baguet, Régis Dufour

► **To cite this version:**

Najib Kacem, Sébastien Hentz, Sébastien Baguet, Régis Dufour. Modélisation non linéaire et optimisation de la gamme dynamique des nanocapteurs résonants. CFM 2009 - 19ème Congrès Français de Mécanique, Aug 2009, Marseille, France. hal-03391361

HAL Id: hal-03391361

<https://hal.science/hal-03391361>

Submitted on 21 Oct 2021

HAL is a multi-disciplinary open access archive for the deposit and dissemination of scientific research documents, whether they are published or not. The documents may come from teaching and research institutions in France or abroad, or from public or private research centers.

L'archive ouverte pluridisciplinaire **HAL**, est destinée au dépôt et à la diffusion de documents scientifiques de niveau recherche, publiés ou non, émanant des établissements d'enseignement et de recherche français ou étrangers, des laboratoires publics ou privés.

From MEMS to NEMS : Modelling and characterization of the non linear dynamics of resonators, a way to enhance the dynamic range

N. KACEM^{a,c}, S. HENTZ^b, S. BAGUET^c, R. DUFOUR^c

a. CEA/LETI /3DSI/DIHS/LCMS, 17 rue des Martyrs 38054 Grenoble, France

b. CEA/LETI /3DSI/D2NT/LSCDP, 17 rue des Martyrs 38054 Grenoble, France

c. LaMCoS, INSA-Lyon, CNRS UMR5259, F69621, France

Résumé :

Le mode de détection fréquentielle a pour avantages d'être extrêmement sensible, a le potentiel d'avoir une large gamme dynamique, peu sensible au bruit, une large gamme de linéarité et une faible consommation électrique. Le principe de détection est basé sur le changement de la fréquence de résonance induit par une modification de la raideur du résonateur. Afin de compenser la détérioration des performances lorsqu'on réduit les tailles des résonateurs des MEMS au NEMS, il s'avère important de trouver des conditions physiques permettant de maximiser le signal de détection et pousser les limites du comportement linéaire. Pour cela, un modèle complet qui prend en compte toutes les sources principales des non-linéarités est nécessaire. Dans ce papier, un modèle analytique sur la dynamique non linéaire de micro et nanorésonateurs ainsi qu'une validation expérimentale sont présentés.

Abstract :

The resonant sensing technique is highly sensitive, has the potential for large dynamic range, good linearity, low noise and potentially low power. The detection principle is based on frequency change that is induced by rigidity changes in the resonator.

In order to compensate the loss of performances when scaling sensors down to NEMS, it proves convenient to find physical conditions in order to maximise the signal variations and to push the limits of the linear behavior. To do so, a comprehensive model including the main sources of nonlinearities is needed. In the present paper, a process, characterization methods and above all an original analytical model are presented.

Mots clefs : MEMS, NEMS, Resonator, non linear dynamics, dynamic range, characterization

1 Introduction

The permanent quest for cost cuts has led to the use of potential "In-IC" compatible thin SOI-based technologies, which imposes drastic size reduction of the sensors. Combined with the need for in-plane actuation for fabrication and design simplicity, this implies a large reduction in detectability. Moreover nonlinearities [1] occur sooner for small structures which reduces their dynamic range.

On the way from MEMS to NEMS, a "small" MEMS resonant accelerometer [2] has been fabricated. The sensor structure has been designed in order to validate process and characterization choices.

This paper deals with the design of the sensitive element : the resonator. Many studies have presented models on the dynamic behavior of MEMS resonators. Some of them are purely analytical [3, 4] but they include coarse assumptions concerning nonlinearities. Other models [5, 6] are more complicated and use numerical simulations which makes them less interesting for MEMS designers. In the present paper, a compact and analytical model including the main sources of nonlinearities is presented and validated thanks to the characterization of the accelerometer sensing element, an electrostatically driven clamped-clamped beam.

2 Model

A clamped-clamped microbeam is considered (Figure 1) subject to a viscous damping with coefficient \tilde{c} per unit length and actuated by an electric load $v(t) = Vdc + Vac \cos(\tilde{\Omega}t)$, where Vdc is the DC polarization voltage, Vac is the amplitude of the applied AC voltage, and $\tilde{\Omega}$ is the excitation frequency.

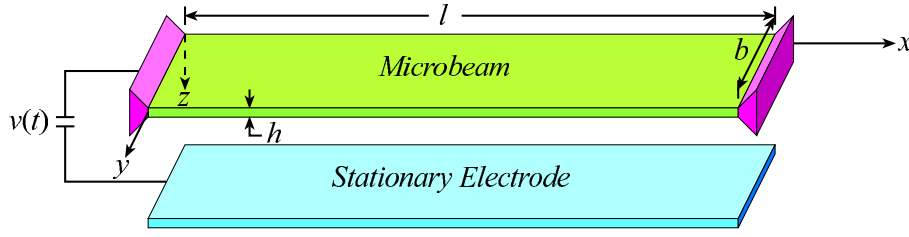


FIG. 1 – Schema of an electrically actuated microbeam

2.1 Equation of motion

The equation of motion that governs the transverse deflection $w(x, t)$ is written as :

$$EI \frac{\partial^4 \tilde{w}(\tilde{x}, \tilde{t})}{\partial \tilde{x}^4} + \rho b h \frac{\partial^2 \tilde{w}(\tilde{x}, \tilde{t})}{\partial \tilde{t}^2} + \tilde{c} \frac{\partial \tilde{w}(\tilde{x}, \tilde{t})}{\partial \tilde{t}} = \left[\tilde{N} + \frac{E b h}{2l} \int_0^l \left[\frac{\partial \tilde{w}(\tilde{x}, \tilde{t})}{\partial \tilde{x}} \right]^2 d\tilde{x} \right] \frac{\partial^2 \tilde{w}(\tilde{x}, \tilde{t})}{\partial \tilde{x}^2} + \frac{1}{2} \varepsilon_0 \frac{b C_n [V_{dc} + V_{ac} \cos(\tilde{\Omega} \tilde{t})]^2}{(g - \tilde{w}(\tilde{x}, \tilde{t}))^2} \quad (1)$$

where \tilde{x} is the position along the microbeam length, E and I are the Young's modulus and moment of inertia of the cross section. \tilde{N} is the applied tensile axial force due to the residual stress on the silicon or the effect of the measurand, \tilde{t} is time, ρ is the material density, h is the microbeam thickness, g is the capacitor gap width, and ε_0 is the dielectric constant of the gap medium. The last term in Equation (1) represents an approximation of the electric force assuming a complete overlap of the area of the microbeam and the stationary electrode including the edge effects by the coefficient C_n [7]. The boundary conditions are :

$$\tilde{w}(0, \tilde{t}) = \tilde{w}(l, \tilde{t}) = \frac{\partial \tilde{w}}{\partial \tilde{x}}(0, \tilde{t}) = \frac{\partial \tilde{w}}{\partial \tilde{x}}(l, \tilde{t}) = 0 \quad (2)$$

2.2 Normalization

For convenience and equations simplicity, we introduce the nondimensional variables :

$$w = \frac{\tilde{w}}{g}, \quad x = \frac{\tilde{x}}{l}, \quad t = \frac{\tilde{t}}{\tau} \quad (3)$$

Where $\tau = \frac{2l^2}{h} \sqrt{\frac{3\rho}{E}}$. Substituting Equation (3) into Equations (1) and (2), we obtain :

$$\frac{\partial^4 w}{\partial x^4} + \frac{\partial^2 w}{\partial t^2} + c \frac{\partial w}{\partial t} - \alpha_2 \frac{[V_{dc} + V_{ac} \cos(\Omega t)]^2}{(1-w)^2} = \left[N + \alpha_1 \int_0^1 \left[\frac{\partial w}{\partial x} \right]^2 dx \right] \frac{\partial^2 w}{\partial x^2} \quad (4)$$

$$w(0, t) = w(1, t) = \frac{\partial w}{\partial x}(0, t) = \frac{\partial w}{\partial x}(1, t) = 0$$

The parameters appearing in Equations (4) are :

$$c = \frac{\tilde{c} l^4}{EI \tau}, \quad N = \frac{\tilde{N} l^2}{EI}, \quad \alpha_1 = 6 \left[\frac{g}{h} \right]^2, \quad \alpha_2 = 6 \frac{\varepsilon_0 l^4}{E h^3 g^3}, \quad \Omega = \tilde{\Omega} \tau \quad (5)$$

2.3 Resolution

A reduced-order model is generated by modal decomposition transforming Equations (4) into a finite-degree-of-freedom system consisting of ordinary differential equations in time. We use the undamped linear mode

shapes of the straight microbeam as basis functions in the Galerkin procedure. To this end, we express the deflection as :

$$w(x, t) = \sum_{k=1}^n a_k(t) \phi_k(x) \quad (6)$$

Where $a_k(t)$ is the k^{th} generalized coordinate and $\phi_k(x)$ is the k^{th} linear undamped mode shape of the straight microbeam, normalized such that $\int_0^1 \phi_k \phi_j = 0$ for $k \neq p$ and governed by :

$$\frac{d^4 \phi_k(x)}{dx^4} = \lambda_k^2 \phi_k(x) \quad (7)$$

$$\phi_k(0) = \phi_k(1) = \phi_k'(0) = \phi_k'(1) \quad (8)$$

Here, λ_k is the k^{th} natural frequency of the microbeam. We multiply Equations (4) by $\phi_k(x)(1-w)^2$, substitute Equation (6) into the resulting equation, use Equation (7) to eliminate $\frac{d^4 \phi_k(x)}{dx^4}$, integrate the outcome from $x = 0$ to 1, and obtain :

$$\begin{aligned} & \ddot{a}_k + c_k \dot{a}_k + \lambda_k^2 a_k - 2 \sum_{j=1}^n \{ \lambda_j^2 a_j^2 + c_j a_j \dot{a}_j + a_j \ddot{a}_j \} \int_0^1 \phi_k \phi_j^2 dx \\ & - \alpha_2 [Vdc + Vac \cos(\Omega t)]^2 \int_0^1 \phi_k dx + \sum_{j=1}^n \{ \lambda_j^2 a_j^3 + c_j a_j^2 \dot{a}_j + a_j^2 \ddot{a}_j \} \int_0^1 \phi_k \phi_j^3 dx \\ & - \sum_{j=1}^n \left\{ N a_j + \alpha_1 a_j^3 \int_0^1 [\phi_j']^2 dx \right\} \int_0^1 \phi_k \phi_j'' dx \\ & + 2 \sum_{j=1}^n \left\{ \alpha_1 a_j^4 \int_0^1 [\phi_j']^2 dx + N a_j^2 \right\} \int_0^1 \phi_k \phi_j \phi_j'' dx \\ & - \sum_{j=1}^n \left\{ \alpha_1 a_j^5 \int_0^1 [\phi_j']^2 dx + N a_j^3 \right\} \int_0^1 \phi_k \phi_j^2 \phi_j'' dx = 0 \end{aligned} \quad (9)$$

Noting that the first mode should be the dominant mode of the system and the other modes are neglected, so it suffices to consider the case $n = 1$. Equation (9) becomes :

$$\begin{aligned} & \ddot{a}_1 + (500.564 + 12.3N)a_1 + (1330.9 + 38.3N)a_1^2 + (927 + 28N + 151\alpha_1) a_1^3 + 471\alpha_1 a_1^4 \\ & + 347\alpha_1 a_1^5 + c_1 \dot{a}_1 + 2.66c_1 a_1 \dot{a}_1 + 1.85c_1 a_1^2 \dot{a}_1 + 2.66a_1 \ddot{a}_1 \\ & + 1.85a_1^2 \ddot{a}_1 = -\frac{8}{3\pi} \alpha_2 [Vdc + Vac \cos(\Omega t)]^2 \end{aligned} \quad (10)$$

To analyse the Equation of motion (10), it proves convenient to invoke perturbation techniques which work well with the assumptions of "small" excitation and damping, typically valid in MEMS resonators. To facilitate the perturbation approach, in this case the method of averaging [8], a standard constrained coordinate transformation is introduced, as given by :

$$\begin{cases} a_1 = A(t) \cos [\Omega t + \beta(t)] \\ \dot{a}_1 = -A(t) \Omega \sin [\Omega t + \beta(t)] \\ \ddot{a}_1 = -A(t) \Omega^2 \cos [\Omega t + \beta(t)] \end{cases} \quad (11)$$

In addition, since near-resonant behavior is the principal operating regime of the proposed system, a detuning parameter, σ is introduced, as given by :

$$\Omega = \omega_n + \varepsilon \sigma \quad (12)$$

Separating the resulting equations and averaging them over the period $\frac{2\pi}{\Omega}$ in the t -domain results in the system's averaged equations, in terms of amplitude and phase, which are given by :

$$\begin{aligned} \dot{A} &= -\frac{1}{2}\epsilon\xi_0 A - \frac{1}{8}\epsilon\xi_2 A^3 - \frac{1}{2}\epsilon\frac{\kappa}{\omega_n} \sin\beta + O(\epsilon^2) \\ A\dot{\beta} &= A\sigma\epsilon - \frac{3}{8}\epsilon\frac{\chi_3}{\omega_n} A^3 - \frac{5}{16}\epsilon\frac{\chi_5}{\omega_n} A^5 + \frac{7}{10}\epsilon\omega_n A^3 + \frac{1}{2}\epsilon\frac{\kappa}{\omega_n} \cos\beta + O(\epsilon^2) \end{aligned} \quad (13)$$

Where $\omega_n = \sqrt{500.564 + 12.3N}$, $\xi_0 = c_1$, $\xi_2 = 1.85c_1$, $\chi_3 = 927 + 28N + 151\alpha_1$, $\chi_5 = 347\alpha_1$ and $\kappa = \frac{16}{3\pi}\alpha_2 VacVdc$.

The steady-state motions occur when $\dot{A} = \dot{\beta} = 0$, which corresponds to the singular points of Equation (13). Thus, the frequency-response equation can be written in its implicit form as :

$$\left(\frac{3}{4\omega_n}\chi_3 A^2 + \frac{5}{8\omega_n}\chi_5 A^4 - \frac{7\omega_n}{5}A^2 - 2\sigma \right)^2 = \left(\frac{\kappa}{A\omega_n} \right)^2 - \left(\xi_0 + \frac{1}{4}\xi_2 A^2 \right)^2 \quad (14)$$

The normalized displacement W_{max} with respect to the gap in the middle of the beam and the drive frequency Ω can be expressed in function of the phase β . Thus, the frequency response curve can be plotted parametrically as shown in Figure 2 for a typical resonator with the following dimensions : $l = 200\mu m$, $b = 4\mu m$, $h = 2\mu m$. The numerical simulations were carried out for an AC voltage $Vac = 5mV$.

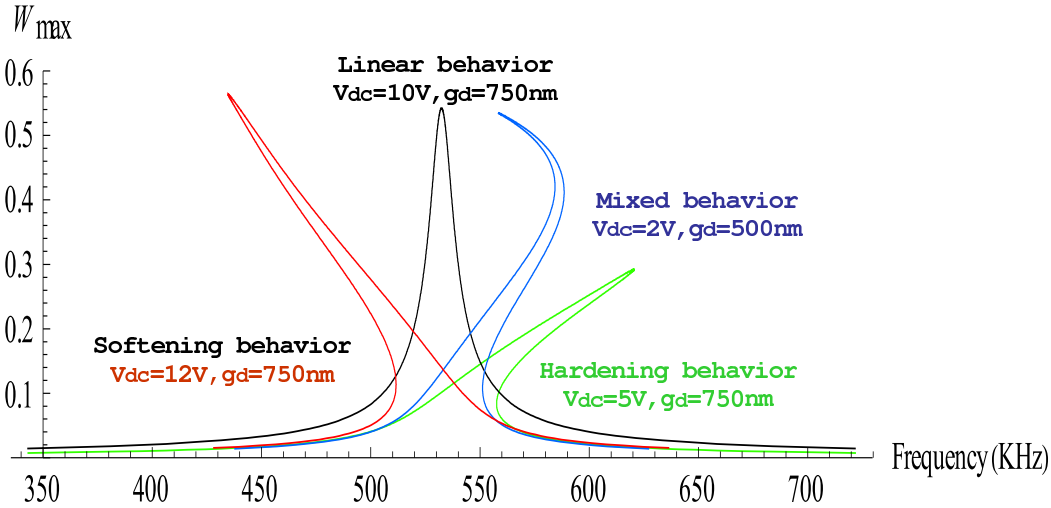


FIG. 2 – Predicted forced frequency responses

This analytical model enables the capture of all the non linear phenomena in the resonator dynamics and describes the competition between the hardening and the softening behaviors. Specific parameters combination permits the compensation of the nonlinearities in order to enhance the dynamic range of the resonator, i.e. its detectability by obtaining a linear behavior (black curve).

2.4 Motional current

Since the system driving electrode/air/resonator constitutes a capacitor (CMEMS), any mechanical motion of the resonator directly translates into an electrical signal. The total capacitive current generated by this system can be expressed as :

$$I_{cap} = -\omega_n Vac \sin[\omega_n t] \int_0^1 \frac{bC_n \epsilon_0}{1 - a_1(t)\phi_1(x)} dx + (Vdc + Vac \cos[\omega_n t]) \int_0^1 \frac{bC_n \epsilon_0 \phi_1(x) a_1'(t)}{(1 - a_1(t)\phi_1(x))^2} dx \quad (15)$$

The total capacitive current was calculated analytically using the results of the reduced order model in displacement and a Taylor series expansion of the capacitance.

3 Manufacturing

The fabrication starts with 200mm SOI wafers ($4\mu\text{m Si}$, $1\mu\text{m SiO}_2$). The use of DUV lithography combined with deep RIE process has allowed 500nm wide gaps and lines. Some low stiffness beams have been designed, so FH-vapor technique had to be improved to enable the release and protection against in-plane sticking. Main steps are shown in Figure 3.




| Schema | Description - Equipment |
|---|---|
|  | Substrate : SOI wafer - SOI $4\mu\text{m P}$ 1-10 mohm.cm - Oxide 1000nm - Bulk $725\mu\text{m P}$ 7-12 ohm.cm |
|  | Photolithography ASM300 (MEMS Level) Dry etching $4\mu\text{m}$ of Si (DRIE). |
|  | Metal deposition and etching HF vapor etching of TEOS HF vapor etching of SiO_2 (Time control) - Lateral release = $5\mu\text{m}$ |

FIG. 3 – Simplified process flow

4 Experimental characterisation

For a start, only the resonant beams were released. The fabricated resonators are electrostatically actuated in-plane. Considering the low capacitance variations and the high motional resistance combined with the important parasitic capacitances, tracking the resonance peak purely electrically is rather awkward. An original SEM set-up was developed, coupled with a real-time in-situ electrical measurement, using an external low noise lock-in amplifier (Figure 4).

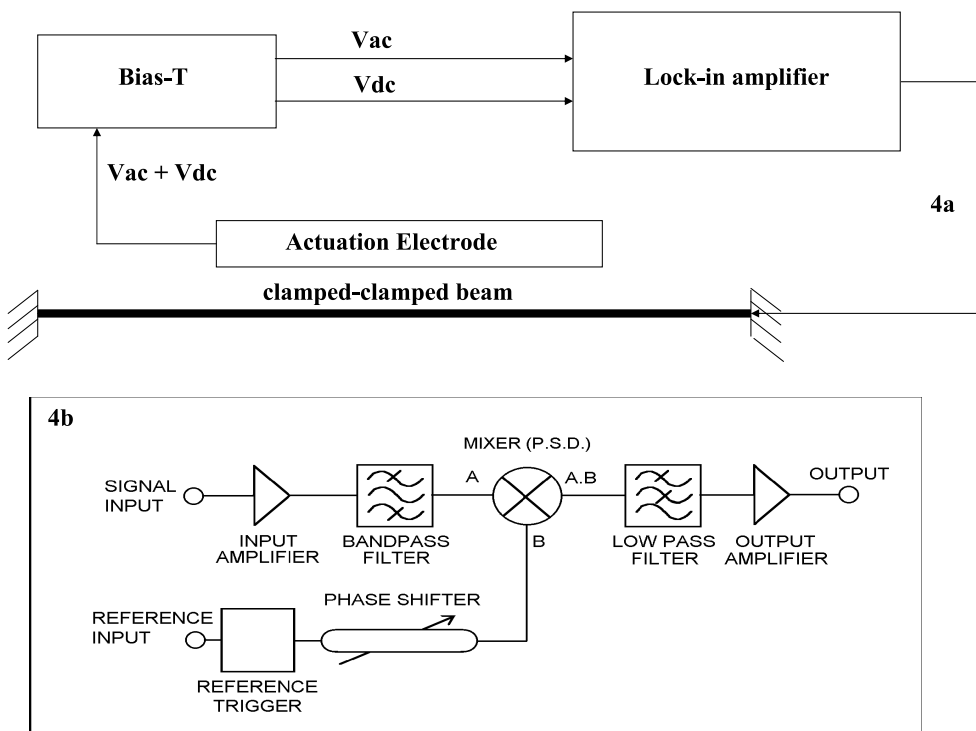


FIG. 4 – (4a) : Connection layout for the electrical characterization. (4b) : Block diagram of a lock-in amplifier.

This set-up allows the simultaneous visualization of the resonance by SEM imaging and the motional current frequency response.

Figure 5 shows some non-linear frequency responses. The residual stress ($\frac{\tilde{N}}{bh} = 15MPa$) and the edge effects coefficient ($C_n = 1.8$) have been measured experimentally and the quality factor is identified for every DC voltage from a linear peak. In addition to these 3 experimental parameters, all what we need to compare the experimental and the model results are the geometric and the electric parameters of the resonator (dimensions : $200\mu m \times 2\mu m \times 4\mu m$, $gap = 750nm$, V_{ac} and V_{dc}). First comparisons are in good agreement with model results.

5 Conclusions

As detailed throughout this work, in-plane MEMS resonators was fabricated and electrically characterized thanks to an original SEM-setup. An analytical model including all the sources of nonlinearities was done in order to predict the resonator behaviors. This analytical model based on a reduced order model obtained with Galerkin procedure and solved via the averaging method, has the advantages to be simple and easy to be implemented for MEMS designers. Moreover, using this model, the dynamic range improvement of MEMS resonators is realizable by compensating the hardening and the softening behaviors. In a future work, the whole sensor will be released and characterized under ac acceleration, so its overall dynamic behavior will be studied. Experimental and model results will be compared, which will complete the model validation.

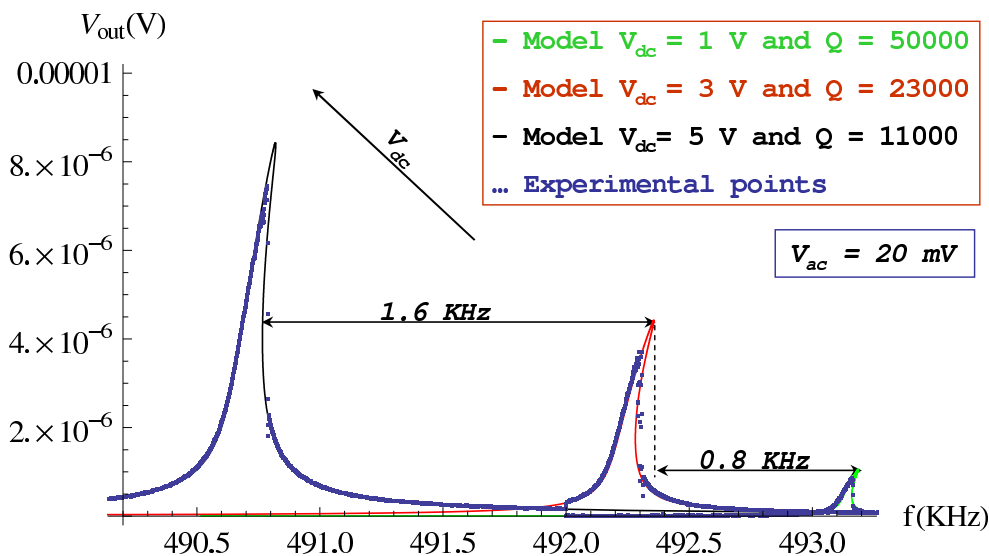


FIG. 5 – Measured and predicted frequency responses

Références

- [1] Roessig T. Integrated MEMS tuning fork oscillators for sensor applications. PhD thesis, University of California, 1998.
- [2] Seshia P. M. R. T. H. R. G. R. S. T., A.A. and S. M. A vacuum packaged surface micromachined resonant accelerometer. *Microelectromech. Syst.*, 11(6), 784–793, 2002.
- [3] Tilmans H. and Legtenberg R. Electrostatically driven vacuum-encapsulated polysilicon resonators part ii. theory and performance. *Sensors and Actuators A*, 45, 67–84, 1994.
- [4] Gui L. R. T. H. F. J., C. and Elwenspoek M. Nonlinearity and hysteresis of resonant strain gauges. *Microelectromech. Syst.*, 7, 122–127, 1998.
- [5] Najar C. S. A. R. E. E.-B. S., F. and Nayfeh A. Dynamic analysis of variable-geometry electrostatic microactuators. *Micromech. Microeng.*, 16, 2449–2457, 2006.
- [6] Nayfeh Y. M., A.H. and Abdel-Rahman E. Dynamic pull-in phenomenon in mems resonators. *Nonlinear Dynamics*, 48, 153–163, 2007.
- [7] Nishiyama H. and Nakamura M. Capacitance of a strip capacitor. *IEEE Trans. Comp., Hybrids, Manuf : Technol.*, 13, 417–423, 1990.
- [8] Nayfeh A. Introduction to perturbation techniques. Wiley, 1981.